



Stern- und
Planetenentstehung
Sommersemester 2020
Markus Röllig

Lecture 11: Protostellar disks and outflows



http://exp-astro.physik.uni-frankfurt.de/star_formation/index.php

VORLESUNG/LECTURE

Raum: Physik - 02.201a

dienstags, 12:00 - 14:00 Uhr

SPRECHSTUNDE:

Raum: GSC, 1/34, Tel.: 47433, (roellig@ph1.uni-koeln.de)

dienstags: 14:00-16:00 Uhr

Nr.	Thema	Termin
1	Observing the cold ISM	21.04.2020
2	Observing Young Stars	28.04.2020
3	Gas Flows and Turbulence Magnetic Fields and Magnetized Turbulence	05.05.2020
4	Gravitational Instability and Collapse	12.05.2020
5	Stellar Feedback	19.05.2020
6	Giant Molecular Clouds	26.05.2020
7	Star Formation Rate at Galactic Scales	02.06.2020
8	Stellar Clustering	09.06.2020
9	Initial Mass Function – Observations and Theory	16.06.2020
10	Massive Star Formation	23.06.2020
11	Protostellar disks and outflows – observations and theory	30.06.2020
12	Protostar Formation and Evolution	07.07.2020
13	Late Stage stars and disks – planet formation	14.07.2020

11 PROTOSTELLAR DISKS AND OUTFLOWS

11.1 OBSERVING DISKS

11.1.1 Dust at optical wavelengths

- Disks do not emit optical light
 - detect disks in scattered starlight
 - detect disks in absorption
 - requires bright, extended background
- e.g. HII regions around massive stars

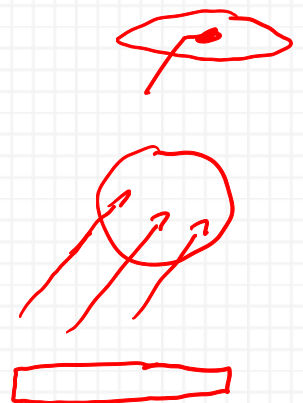
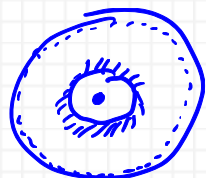


Abbildung 1 Three disks (proplyd) in the Orion Nebula seen in absorption against the nebula using the HST.
<http://hubblesite.org/newscenter/archive/releases/1995/45/image/>

- advantage: excellent spatial resolution (scale in Fig 1 ~ 100 AU)
- requires favorable geometry
- observation only possible once the dusty envelope is gone (later stage of disk evolution)

11.1.2 Dust emission in the Infrared and Sub-mm



- Warm dust near the central star
- If the star is also visible => dust cannot be in a spherical shell => disk
- Few observations where disks are resolved

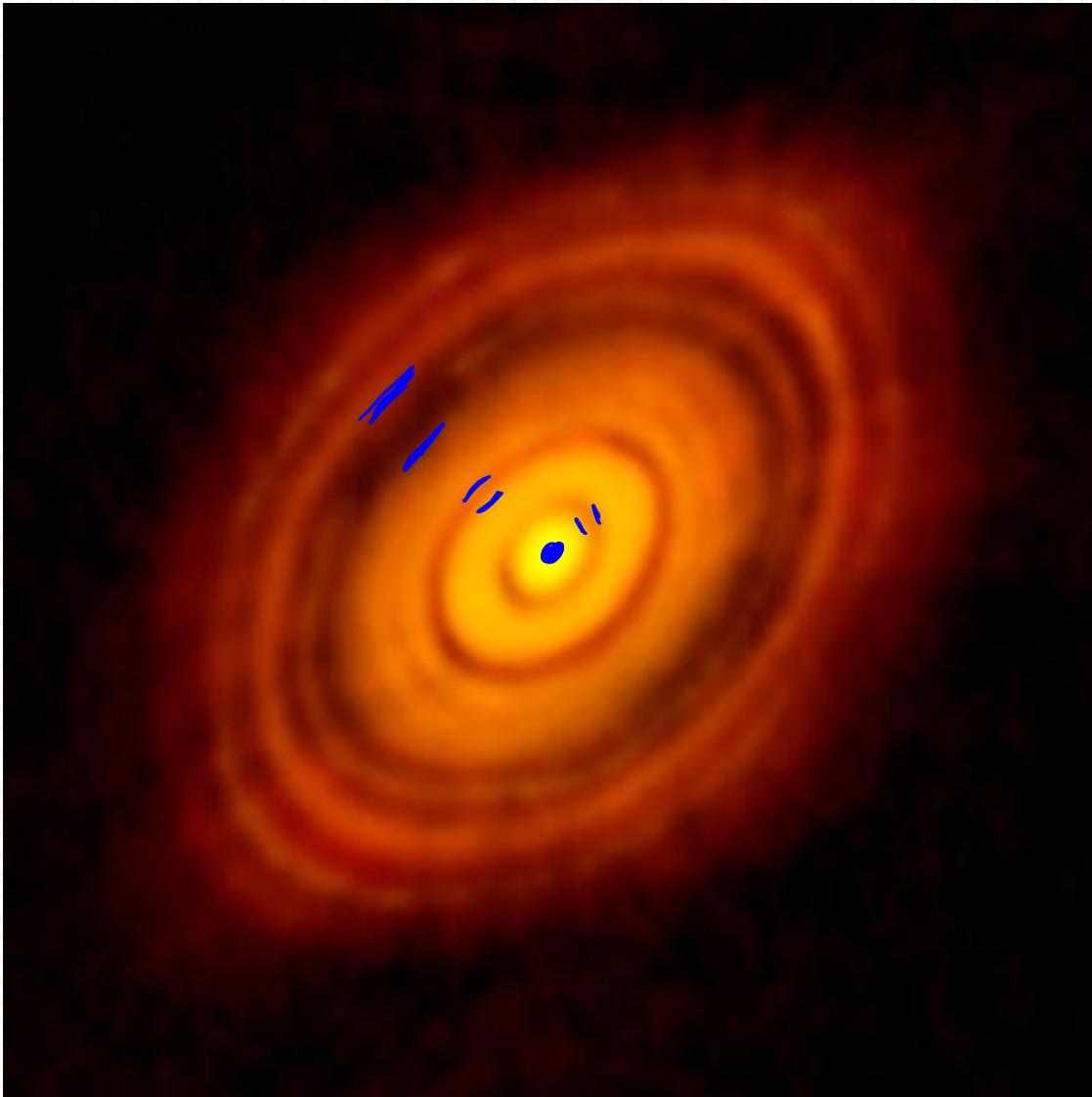


Abbildung 2 An ALMA image of the disk around the young star HL Tau. The image shows dust continuum emission. Image from <https://public.nrao.edu/static/pr/planet-formation-alma.html>

Expected emission of a disk:

thin disk of surface density $\Sigma(\omega)$ and temperature $T(\omega)$ beginning at radius ω_0 and extending up to radius ω_1

dust opacity κ_λ , inclination angle θ , received flux:

projected ring area

$$2\pi\omega \cos\theta d\omega$$

distance D

$$F_\lambda = \int I_\lambda d\Omega$$

$$F_\lambda = \frac{2\pi \cos\theta}{D^2} \int I_\lambda(\omega) \omega d\omega$$

$$\tau_\lambda = \frac{\kappa_\lambda \Sigma}{\cos\theta}$$

$$F_\lambda = \frac{2\pi \cos\theta}{D^2} \int_{\omega_0}^{\omega_1} B_\lambda(T) \left[1 - \exp\left(-\frac{\kappa_\lambda \Sigma}{\cos\theta}\right) \right] \omega d\omega$$

$$I_\lambda = B_\lambda(T) [1 - e^{-\tau_\lambda}]$$

Fitting an observation F_λ to the disk model requires $\Sigma(\omega)$ and $T(\omega)$ (and κ_λ)

- complicated models of disk
 - temperature (heating, cooling)
 - density
 - chemical structure

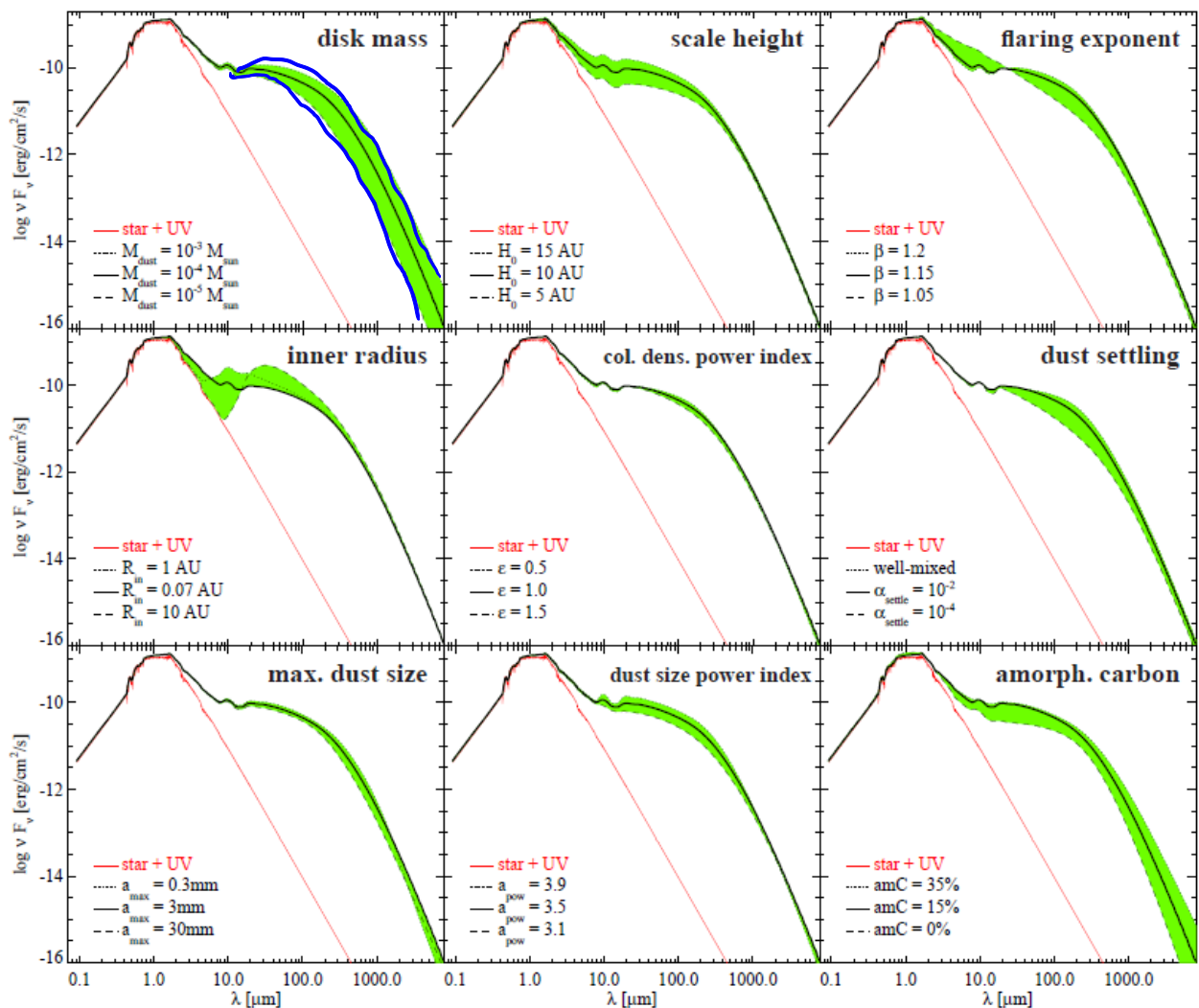
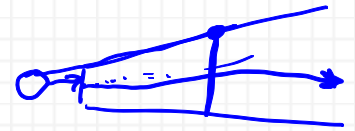


Fig. 8. Effect of dust and disk parameters on model SED at distance 140 pc and inclination 45°. The thick full black line is the reference model (identical in every part figure), whereas the green shaded area indicates the effect of a single parameter on the SED, where the dashed and dotted lines correspond to the changed parameter values as annotated. Top row: dust mass M_{dust} , scale height H_0 , and flaring exponent β . 2nd row: inner radius R_{in} , column density powerlaw index ϵ , and dust settling parameter α_{settle} . 3rd row: maximum grain size a_{max} , dust size powerlaw index α_{pow} , and volume ratio of amorphous carbon. The dependencies of the SED on the tapering-off radius R_{tap} (not shown), on the outer radius R_{out} (not shown), and on the minimum dust particle size a_{min} (not shown) are less than the one shown for ϵ .

Abbildung 3 Woitke et al. 2016

OPTICAL THICK LIMIT

$$\tau_\lambda = \frac{\kappa_\lambda \Sigma}{\cos \theta} \gg 1 \Rightarrow \exp(-\tau_\lambda) \rightarrow 0$$

Σ dependence removed in thick limit!

$$F_\lambda = \frac{4\pi \cos \theta}{D^2} \frac{hc^2}{\lambda^5} \int_{\omega_0}^{\omega_1} \frac{\omega}{\exp[hc/(k_B T)] - 1} d\omega$$

assume $T = T_0 (\omega/\omega_0)^{-q}$ and substitute $x = \left(\frac{hc}{\lambda k_B T_0}\right)^{1/q} \frac{\omega}{\omega_0}$

$$F_\lambda = \frac{4\pi \cos \theta}{D^2} \frac{hc^2}{\lambda^5} \left(\frac{\omega_0}{x_0}\right)^2 \int_{x_0}^{x_1} \frac{x}{\exp[x^q] - 1} dx$$

$$F_\lambda = \frac{4\pi \cos \theta}{D^2} \frac{hc^2}{\lambda^5} \left(\frac{hc}{\lambda k_B \omega_0^q T_0}\right)^{-2/q} \int_{x_0}^{x_1} \frac{x}{\exp[x^q] - 1} dx$$

Integrating from $x_0 = 0$ to $x_1 = \infty$

$$\lambda F_\lambda \propto \lambda^{(2-4q)/q}$$

At small wavelength this can be inverted and the temperature law can be deduced.

OPTICAL THIN LIMIT

@long wavelengths (FIR, sub-mm), outer disk with lower Σ

$$1 - \exp\left(-\frac{\kappa_\lambda \Sigma}{\cos \theta}\right) \approx \frac{\kappa_\lambda \Sigma}{\cos \theta}$$

$$F_\lambda = \frac{2\pi}{D^2} \int_{\omega_0}^{\omega_1} B_\lambda(T) \kappa_\lambda \Sigma \omega d\omega$$

inclination becomes irrelevant. Assuming RJ limit

$$B_\lambda(T) \approx \frac{2ck_B T}{\lambda^4}$$

$$F_\lambda = \frac{4\pi ck_B \kappa_\lambda \Sigma}{D^2 \lambda^4} \int_{\omega_0}^{\omega_1} T \omega d\omega$$

λ -dependence outside of integral

assuming:

$$\lambda F_\lambda \propto \lambda^{-3-\beta}$$

$$\kappa_\lambda \propto \lambda^{-\beta}$$

The sub-mm SED tells us about the wavelength dependence of the dust opacity!

ISM: $\beta \approx 2$ in the diffuse ISM, $\beta \approx 1$ in the dense ISM

reduction in β indicates grain growth

but also transition from optically thick to thin causes the SED to flatten!

11.1.3 Disks in molecular lines

Line emission also reveals kinematics!

e.g. truncation radius of disk from max. rotation velocity

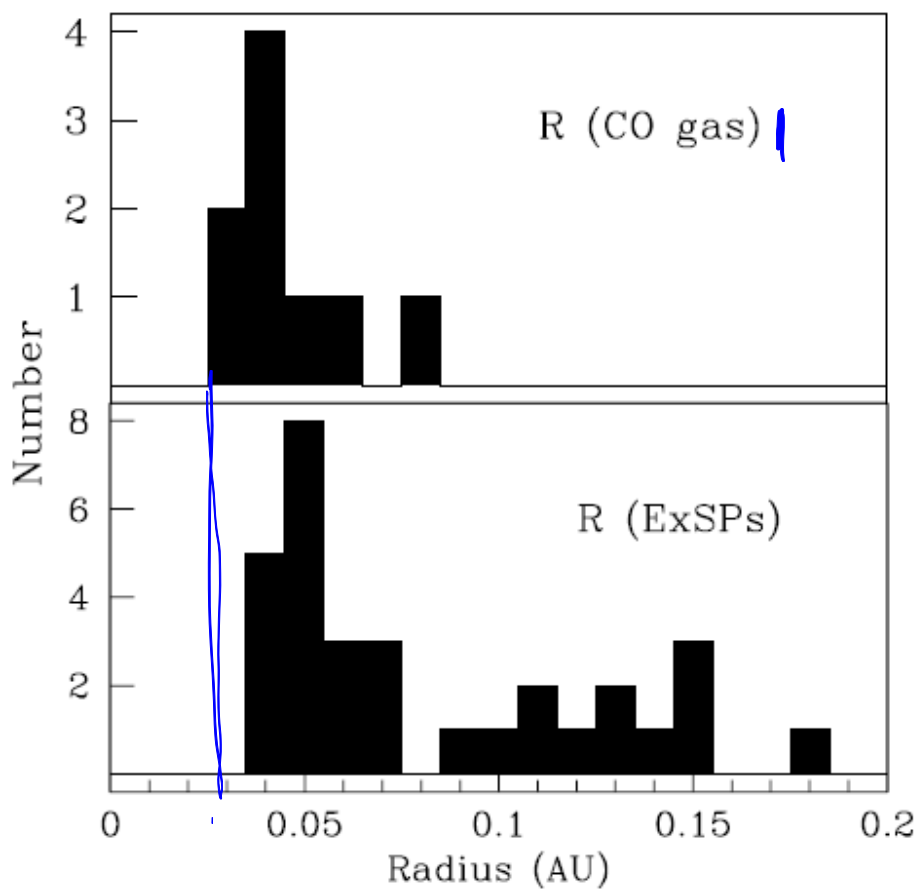
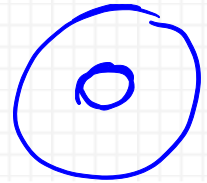


Fig. 3.— The distribution of gaseous inner radii, measured with the CO fundamental transitions, compared to the distribution of orbital radii of short-period extrasolar planets. A minimum planetary orbital radius of ~ 0.04 AU is similar to the minimum gaseous inner radius inferred from the CO emission line profiles.

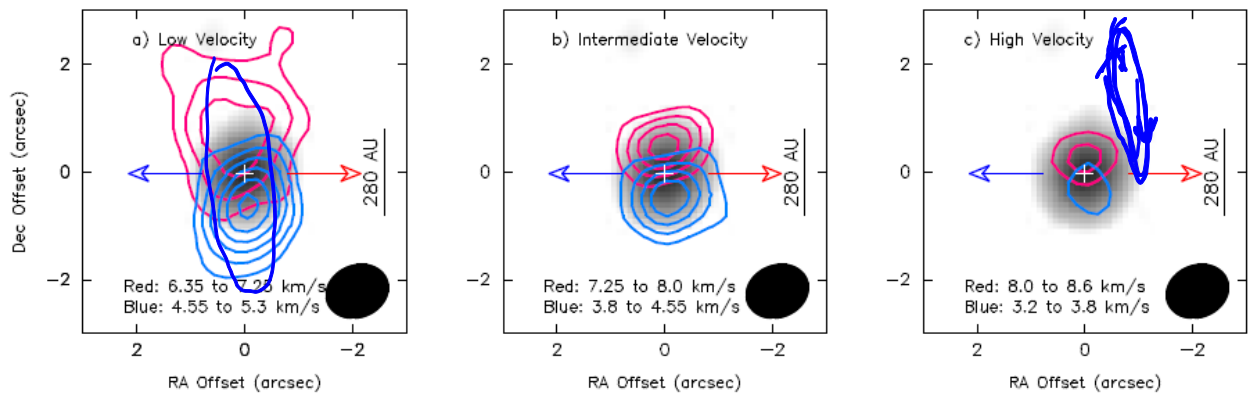


FIGURE 3. ^{13}CO emission from the disk around L1527 exhibiting a Keplerian rotation signature. The CARMA 1.3 mm continuum image is shown (grayscale) with the red and blue contours showing ^{13}CO emission integrated at low velocities (a), intermediate velocities (b), and high velocities (c). The white cross in all panels marks the location of the protostar. The blue and red-shifted emission centroids show a clear signature of rotation on the size-scale of the protostellar disk and no extension of emission along the outflow. The low-velocity emission likely includes contributions from the envelope, while the intermediate to high-velocity emission is dominated by the disk. The low velocity range is from 6.35 km s^{-1} to 7.25 km s^{-1} and 4.55 km s^{-1} to 5.3 km s^{-1} ; the intermediate velocity range is from 7.25 km s^{-1} to 8.0 km s^{-1} and 3.8 km s^{-1} to 4.55 km s^{-1} ; the high velocity range is from 8.0 km s^{-1} to 8.6 km s^{-1} and 3.2 km s^{-1} to 3.8 km s^{-1} . The contours start and increase in intervals 3 times noise level (σ) where $\sigma = 0.85 \text{ K km s}^{-1}$ (red) and 0.75 K km s^{-1} (blue). The angular resolution of these data are given by the ellipse in the lower right corners, $1.1'' \times 0.95''$.

Abbildung 5 Tobin et al. 2012

Keplerian orbits are fastest in the inner disk

11.2 OBSERVATIONS OF OUTFLOWS

11.2.1 Outflows in the optical

First detected in the optical in the 1950s (Herbig & Haro)

Small patches of optical emission (continuum & lines)

Interpretation: fast shock (-> ionization, therefore $\text{H}\alpha$ emission) and up/downstream we find neutral, warm material (emission lines)

1970: knots are aligned in linear structures (bi-polar) with bow shocks at the head of the jets

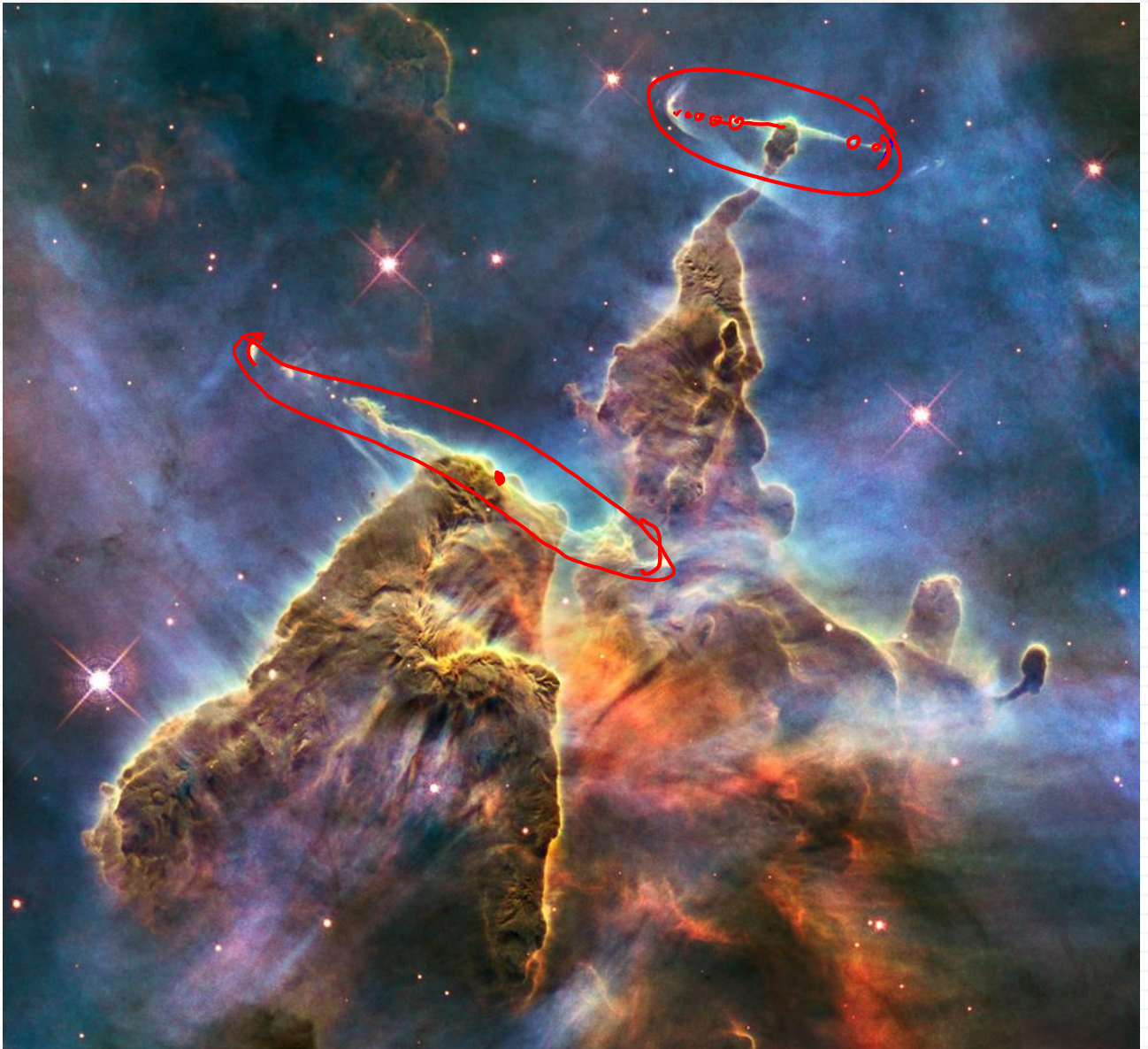


Abbildung 6 Herbig-Haro jets imaged with the Hubble Space Telescope. Two jets are visible; one is at the tip of the "pillar" near the top of the image, and another is near the edge of the structure in the middle-left part of the image. Bow shocks from the jets are clearly visible. Taken from <http://hubblesite.org/newscenter/archive/releases/2010/13/image/a/>.

knots: locations where the jet encountered a dense ISM region (producing strong shocks) or where variations of the velocity or mass flux feeding the jet caused internal shocks (then knots are symmetrically w.r.t. to the both bipolar jets).

HH jets move typically with few 100s km s^{-1} . Visible spatial variation on timescales of 10 years.

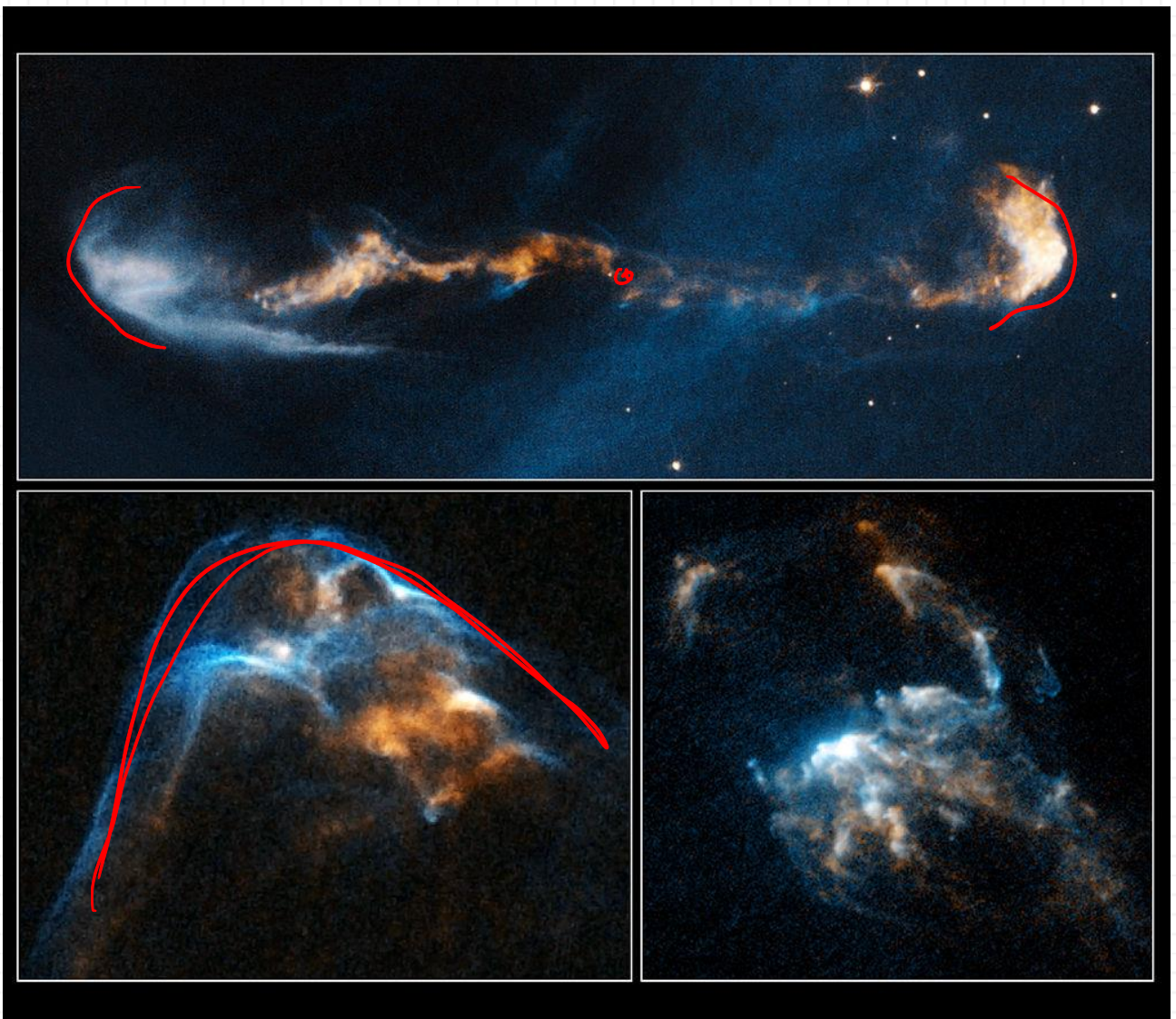


Abbildung 7 The glowing, clumpy streams of material shown in these NASA/ESA Hubble Space Telescope images are the signposts of star birth. Ejected episodically by young stars like cannon salvos, the blobby material zips along at more than 700 000 kilometres per hour. The speedy jets are confined to narrow beams by the powerful stellar magnetic field. Called Herbig-Haro or HH objects, these outflows have a bumpy ride through space. When fast-moving blobs collide with slower-moving gas, bow shocks arise as the material heats up. Bow shocks are glowing waves of material similar to waves produced by the bow of a ship ploughing through water. In HH 2, at lower right, several bow shocks can be seen where several fast-moving clumps have bunched up like cars in a traffic jam. In HH 34, at lower left, a grouping of merged bow shocks reveals regions that brighten and fade over time as the heated material cools where the shocks intersect. In HH 47, at top, the blobs of material look like a string of cars on a crowded motorway, which ends in a chain-reaction accident. The smash up creates the bow shock, left. These images are part of a series of time-lapse movies astronomers have made showing the outflows' motion over time. The movies were stitched together from images taken over a 14-year period by Hubble's Wide Field Planetary Camera 2. Hubble followed the jets over three epochs: HH 2 from 1994, 1997, and 2007; HH 34 from 1994, 1998, and 2007; and HH 47 from 1994, 1999, and 2008. The outflows are roughly 1350 light-years from Earth. HH 34 and HH 2 reside near the Orion Nebula, in the northern sky. HH 47 is located in the southern constellation of Vela.

Estimated momentum flux: $10^{-6} - 10^{-3} M_{\odot} \text{ km s}^{-1} \text{ yr}^{-1}$ (very uncertain)

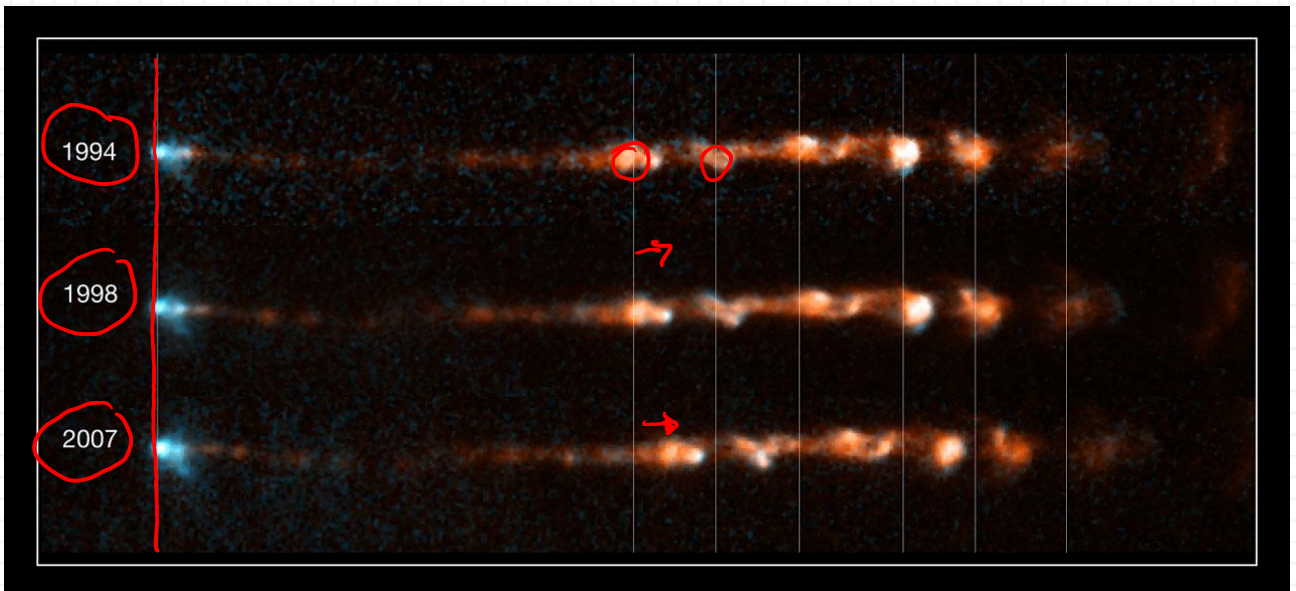


Abbildung 8 HH34, Credit: NASA, ESA, and P. Hartigan (Rice University)

11.2.2 Outflows in the radio

optical & near-IR: traces strong shock heating

molecular lines show that narrow optical jets are accompanied by a much wider-angle, slower-moving and more massive molecular outflow

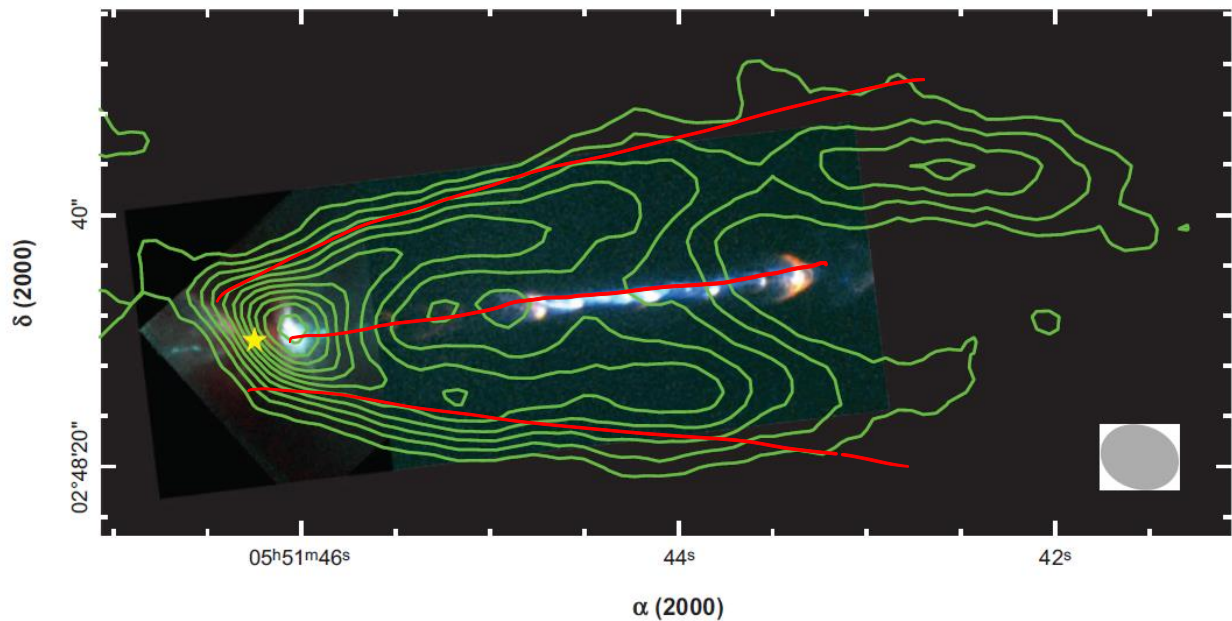


Abbildung 9 McKee & Ostriker 2007: The HH 111 jet and outflow system. The color scale shows a composite Hubble Space Telescope image of the inner portion of the jet (WFPC2/visible) and the stellar source region (NICMOS/IR) (Reipurth et al. 1999). The green contours show the walls of the molecular outflow using the $v = 6 \text{ km s}^{-1}$ channel map from the CO $J = 1-0$ line, obtained with BIMA (Lee et al. 2000). The yellow star marks the driving source position, and the grey oval marks the radio image beam size; the total length of the outflow lobe shown is $\approx 0.2 \text{ pc}$.

Molecular lines show: large masses of mol. gas moving at $\sim 10 \text{ km s}^{-1}$.

These component carry bulk of outflow momentum:

$$10^{-4} - 10^{-1} M_{\odot} \text{ km s}^{-1} \text{ yr}^{-1}$$

Interpretation: not directly ejected material but ambient gas swept up by the jets.

11.3 THEORY

11.3.1 Disk Formation

11.3.1.1 *The Angular Momentum of Protostellar Cores*

Measure the angular momentum by line observations:

Ω : angular velocity of the rotation, I : moment of inertia of the core

ratio of E_{kin} in rotation to E_{grav} \rightarrow dimensionless measure β

$$\beta = \frac{(1/2)I\Omega^2}{\alpha GM^2/R}$$

for sphere of uniform density ρ

$$\beta = \frac{1}{4\pi G\rho} \Omega^2 = \frac{\Omega^2 R^3}{3GM}$$

Typical observed values: few percent (Goodman et al. 1993)

Cores are not primarily supported by rotation

11.3.1.2 *Rotating Collapse: The Hydrodynamic Case*

Fluid element at distance r_0 from axis of rotation (assume in equatorial plane)

Initial angular momentum: $j = r_0^2 \Omega$ (no pressure assumed)

Energy and j remains constant. At closest approach to central star r_{min} its velocity is max

$$v_{max} = \sqrt{2GM_*/r_{min}} \quad j = r_{min} v_{max}$$

$$r_{min} = \frac{r_0^4 \Omega^2}{GM_*} = \frac{4\pi\rho\beta r_0^4}{M_*}$$



(radius at which infalling material must go into the disk because it cannot come any closer)

$$M_* = (4/3)\pi\rho r_0^3$$

$$r_{min} = 3\beta r_0$$

Cores of ~ 0.1 pc size should become rotationally flattened at radii of several hundred AU

11.3.1.3 Rotating Collapse: The MHD Case

Effect of magn. fields: core contracts, rotation wants to spin up, twists magn. field lines, tension force that opposes rotation and tries to keep the core rotating like a solid body.

Cylindrical coordinates (ω, ϕ, z) , fluid element with velocity v_ϕ in ϕ direction

Magnetic field through fluid element: $\mathbf{B} = (B_\omega, B_\phi, B_z)$

poloidal component: $\mathbf{B}_p = (B_\omega, B_z)$, toroidal component B_ϕ

fluid and magn. field: axisymmetric

Lorentz force on fluid element

poloidal gradient

$$\mathbf{f} = \frac{1}{4\pi} [(\nabla \times \mathbf{B}) \times \mathbf{B}]$$

$$\nabla_p = (\partial/\partial\omega, \partial/\partial z)$$

$$= \frac{1}{4\pi} \left[\frac{B_\omega}{\omega} \frac{\partial(\omega B_\phi)}{\partial\omega} + B_z \frac{\partial B_\phi}{\partial z} \right] \hat{\phi}$$

$$= \frac{1}{4\pi} \mathbf{B}_p \cdot \nabla_p (\omega B_\phi) \hat{\phi}$$

rate of change of momentum associated with the Lorentz force:

$$\frac{\partial}{\partial t} (\rho \mathbf{v}) = \mathbf{f}$$

ϕ component and multiplication with $\omega \rightarrow$ angular momentum

$$\frac{\partial}{\partial t}(\rho v_\phi \omega) = \frac{1}{4\pi} \mathbf{B}_p \cdot \nabla_p(\omega B_\phi)$$

left: time rate of change of angular momentum per unit volume $\rho v_\phi \omega$

right: torque per unit volume exerted by the magnetic field

magnetic braking time:

$$t_{br} \approx \frac{(\rho v_\phi \omega)}{\frac{\partial}{\partial t}(\rho v_\phi \omega)} = \frac{4\pi \rho v_\phi \omega}{\mathbf{B}_p \cdot \nabla_p(\omega B_\phi)}$$

Consider a collapsing fluid element that is trying to rotate with Keplerian velocity:

$$v_\phi = \sqrt{\frac{GM}{\omega}} \approx \sqrt{(4\pi/3)G\rho\omega^2}$$

$$t_{br} \approx \frac{(4\pi\rho)^{3/2} G^{1/2} \omega^2}{\mathbf{B}_p \cdot \nabla_p(\omega B_\phi)}$$

Assume: poloidal and toroidal components are comparable, characteristic length scale on which field varies is , i.e. fairly smooth

Then

$$\mathbf{B}_p \cdot \nabla_p(\omega B_\phi) \sim B^2$$

dropping all constants of order unity

Alfven speed

$$t_{br} \sim \frac{G^{1/2} \rho^{3/2} \omega^2}{B^2} \sim \frac{(G\rho)^{1/2} \omega^2}{v_A^2} \sim \frac{t_{cr}^2}{t_{ff}}$$

$$v_A = B/\sqrt{4\pi\rho}$$

$$t_{cr} = \omega/v_A$$

If the cloud starts with energetic equipartition: $t_{cr} \sim t_{ff}$

so $t_{br} \sim t_{cr}$

Even a marginally wound up magn. field is capable of stopping Keplerian rotation in a time scale comparable to the collapse or crossing time.

If the magn. field is strong enough this prevents disk formation at all!

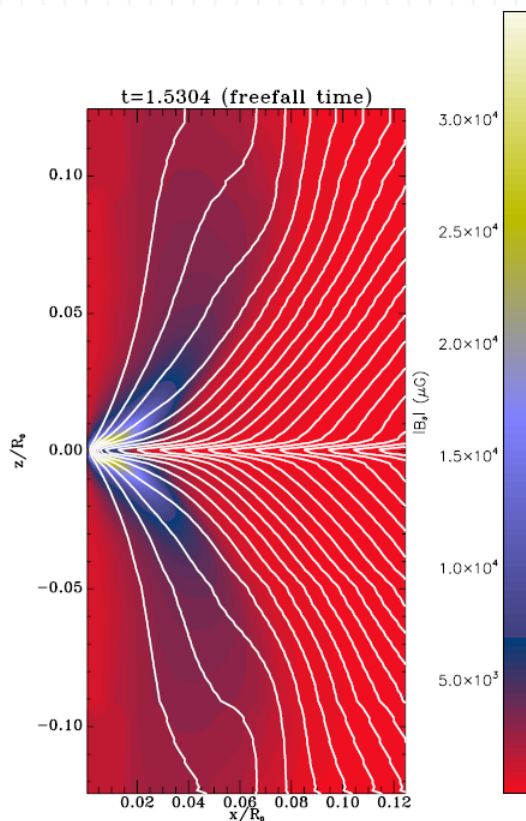


Fig. 13. Structure of the azimuthally averaged magnetic field in the model having $\mu = 2$ at time $t = 1.5304\tau_{ff}$. The solid lines display the poloidal magnetic field lines. They are overlotted on a snapshot of the toroidal magnetic field strength.

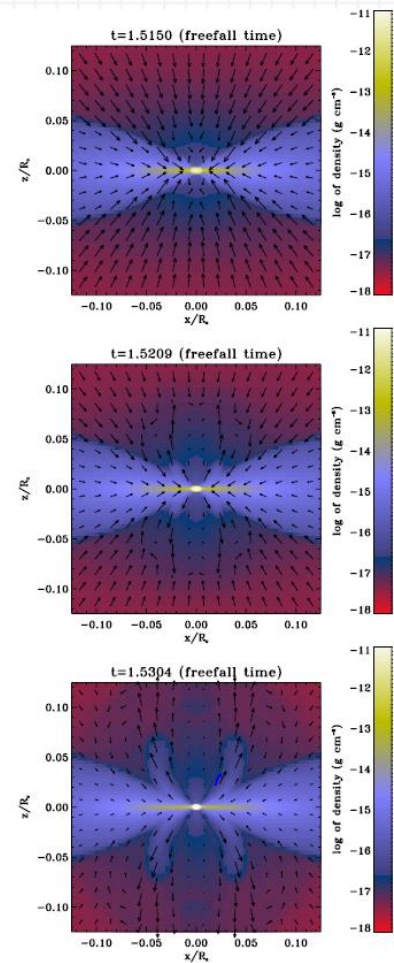


Fig. 12. Case $\mu = 2$. Density and velocity fields in the xz plane.

11.3.1.4 The Magnetic Braking Problem

Problem: It naively seems like magnetic fields should prevent disks from forming at all, but we observe that they do.

We even observe disks present in class 0 sources, where the majority of the gas is still in the envelope.

- Could Ion-Neutral drift offer a way out?
 - I-N-drift allows gas to decouple from magn. field on scales below $L_{AD} \sim 0.05 pc$ ↓ Disk formation below this scale?
 - Simulations suggest that this does not work.
 - I-N drift → gas flux released from the gas.

- I-N-drift builds up flux tubes near the star
- this flux tubes prevent disk formation

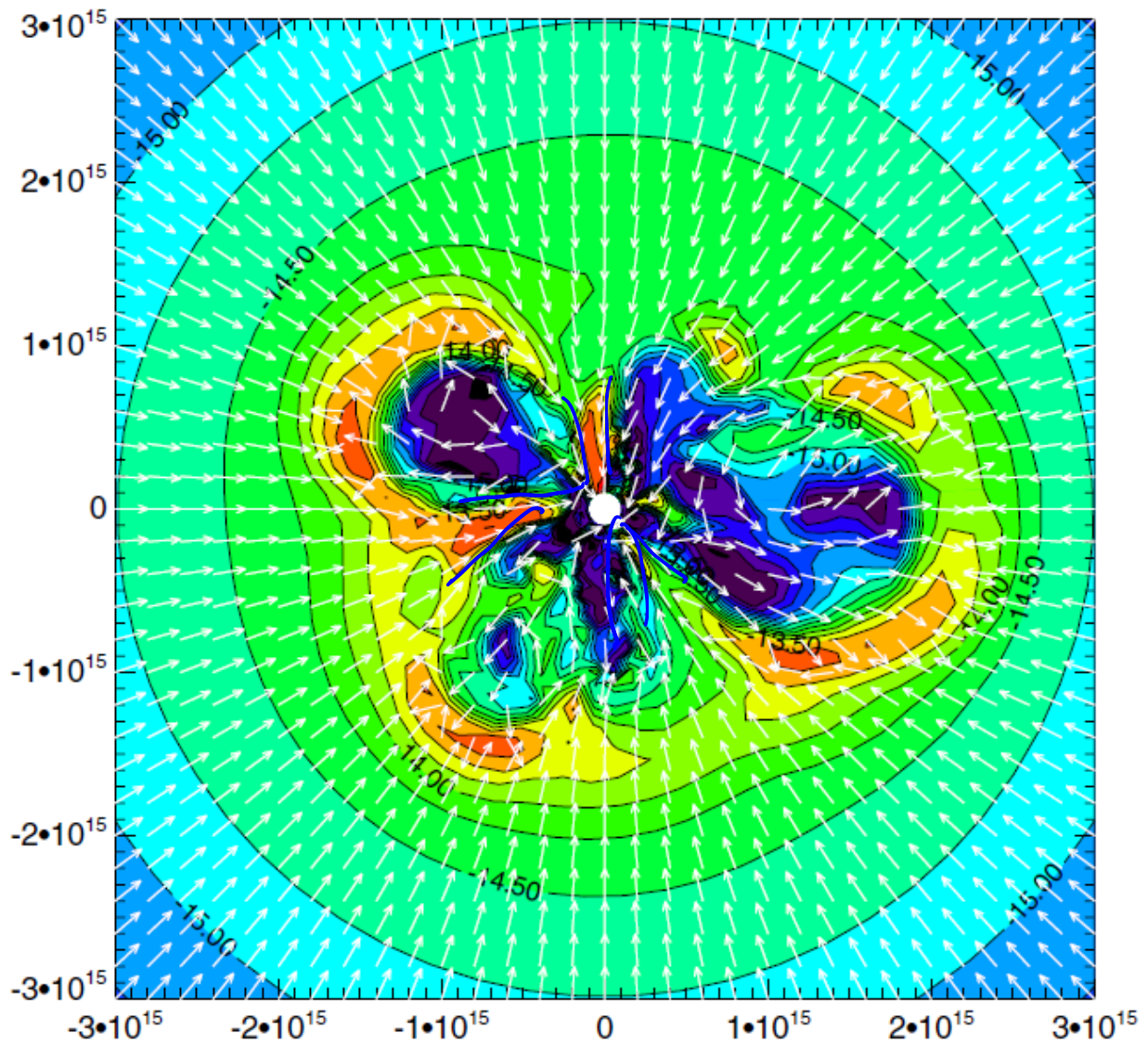


Abbildung 10 Results from a simulation of magnetized rotating collapse including the effects of ion-neutral drift and Ohmic dissipation (Krasnopolsky et al., 2012). Lengths on the axes are in units of cm. Colors and contours show the density in the equatorial plane, on a logarithmic scale from $10^{-16.5}$ to $10^{-12.5}$ g cm⁻³. Arrows show velocity vectors.

- Misalignment between rotation axis and magnetic field
 - i.e. turbulence in the collapsing gas
 - turbulence bends and misaligns magnetic field lines
 - efficiency of magnetic braking is greatly reduced
- Problem still not fully solved

11.3.2 Disk Evolution

Given that disks exist, we wish to understand how they evolve, and how they accrete onto their parent stars.

11.3.2.1 Steady Thin Disk

Consider: Thin disk ($z = 0$, only), Σ surface density, Ω angular velocity, cylindrical symmetric (only function of radius r)

orbital velocity $v_\phi = r\Omega$, radial velocity $v_r (< v_\phi, \text{ so gas can accrete})$

equation of mass conservation:

$$\frac{\partial}{\partial r} \rho + \nabla \cdot (\rho \mathbf{v}) = \frac{\partial}{\partial t} \rho + \frac{1}{r} \frac{\partial}{\partial r} (r \rho v_r) = 0$$

$$\rho = \Sigma \delta(z)$$

drop components of divergence in z and ϕ directions

$$\frac{\partial}{\partial t} \Sigma + \frac{1}{r} \frac{\partial}{\partial r} (r \Sigma v_r) = 0$$

integrate over z

$$\frac{\partial}{\partial t} \Sigma + \frac{1}{2\pi r} \frac{\partial}{\partial r} \dot{M} = 0$$

$$\dot{M} = -2\pi r \Sigma v_r$$

Navier-Stokes equation

$$\rho \left(\frac{\partial}{\partial t} \mathbf{v} + \mathbf{v} \cdot \nabla \mathbf{v} \right) = -\nabla p - \rho \nabla \psi + \nabla \cdot \mathbf{T}$$

p : pressure

ψ : grav. potential

\mathbf{T} : viscous stress tensor

integrate over z

$$\Sigma \left[\frac{\partial}{\partial t} v_\phi + \frac{v_r}{r} \frac{\partial}{\partial r} (r v_\phi) \right] = \int \frac{1}{r^2} \frac{\partial}{\partial r} (r^2 T_{r\phi}) dz$$

ϕ derivatives vanish because of symmetry

multiply by $2\pi r^2$

$$2\pi r \Sigma \left[\frac{\partial}{\partial t} j + v_r \frac{\partial}{\partial r} j \right] = \int \frac{\partial}{\partial r} (2\pi r^2 T_{r\phi}) dz = \frac{\partial}{\partial r} \mathcal{T}$$

$j = r v_\phi$: angular momentum per unit mass

$$\mathcal{T} = 2\pi r \int r T_{r\phi} dz$$

$2\pi r \Sigma$: mass per unit radius in a thin ring, $2\pi r \Sigma j$: angular momentum in a thin ring, \mathcal{T} : torque exerted on the ring due to viscosity.

Suppose we look for solutions of this equation in which the angular momentum per unit mass at a given location stays constant: $\partial j / \partial t = 0$

This will be the case, for example, of a disk where the azimuthal motion is purely Keplerian at all times. In this case the evolution equation just becomes

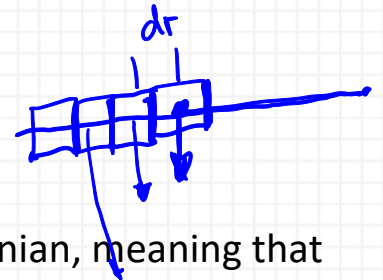


$$-\dot{M} \frac{\partial j}{\partial r} = \frac{\partial \mathcal{T}}{\partial r}$$

the accretion rate \dot{M} is controlled by the rate at which viscous torques remove angular momentum from material closer to the star and give it to material further out.

In case of Keplerian rotation: $j = \sqrt{GM}r$

relationship: accretion rate-viscous torque



- We will assume that the gas in the disk is Newtonian, meaning that the viscous stress is proportional to the rate of strain in the fluid.
- We want to know $T_{r\phi}$, meaning the force per unit area in the ϕ direction, exerted on the radial face of a fluid element.
- Consider an observer in a frame comoving with the orbiting fluid at some particular distance r from the star
- Consider a fluid element that is initially on the same radial ray as the observer, but a distance dr further from the star.
- If the rotation is solid body, then the fluid element and the observer will always lie on the same radial ray, so there is no strain, and there will be no viscous stress.
- If there is differential rotation, such that the fluid further the star has a longer orbital period (as we expect for Keplerian motion), the fluid element will gradually fall behind the observer. This represents a strain in the fluid.

How quickly does the element fall behind?



difference in angular momentum: $d\Omega = (d\Omega/dr)dr$

difference in spatial velocity: $r(d\Omega/dr)dr$

rate of strain $r(d\Omega/dr)dr/dr = r(d\Omega/dr)$

Viscous stress: rate of strain times the dynamic viscosity:

$$T_{r\phi} = \mu r \frac{d\Omega}{dr} = \rho \nu r \frac{d\Omega}{dr} \quad \text{kinematic viscosity}$$

$$\nu = \mu / \rho$$

$$\mathcal{T} = 2\pi r \int r T_{r\phi} dz = 2\pi r^3 \Sigma \nu r \frac{d\Omega}{dr}$$

Assume Keplerian rotation: $j = \sqrt{GM r}$, $\Omega = \sqrt{GM/r^3}$

$$\frac{\partial}{\partial t} \Sigma - \frac{1}{2\pi r} \frac{\partial}{\partial r} \dot{M} = 0$$

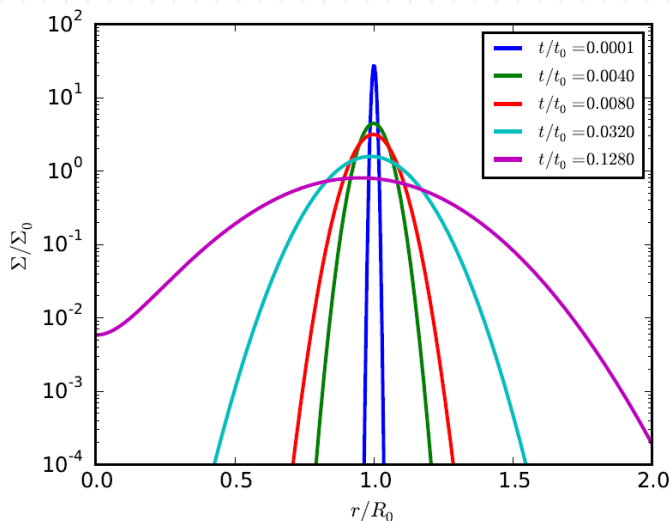
$$-\dot{M} \frac{\partial j}{\partial r} = \frac{\partial \mathcal{T}}{\partial r}$$

gives:

$$\frac{\partial \Sigma}{\partial t} = \frac{3}{r} \frac{\partial}{\partial r} \left[r^{\frac{1}{2}} \frac{\partial}{\partial r} \left(\nu \Sigma r^{\frac{1}{2}} \right) \right] \quad \frac{\partial}{\partial t} \approx \frac{\partial^2}{\partial r^2}$$

$$\left[v_r = -\frac{3}{\Sigma r^{\frac{1}{2}}} \frac{\partial}{\partial r} \left(\nu \Sigma r^{\frac{1}{2}} \right) \right]$$

$\frac{\partial}{\partial t} \propto \frac{\partial^2}{\partial r^2}$ diffusion eq., if we start with a sharply peaked Σ , say a surface density that looks like a ring, viscosity will spread it out.



Analytic solution for the viscous ring of material with constant kinematic viscosity ν . At time $t = 0$, the column density distribution is $\Sigma = \Sigma_0 \delta(r - R_0)$. Colored lines show the surface density distribution at later dimensionless times, as indicated in the legend. (Pringle (1981)).

How quickly do rings spread, and does mass move inward?

Assume: Σ and ν are \sim constant

$$\frac{dJ}{dr} = -3\pi\Sigma\nu \frac{dj}{dr}$$

$$\dot{M} = 3\pi\Sigma\nu$$

$$v_r = -\frac{3\nu}{2r}$$

The time required for a given fluid element to reach the star, therefore, is:

$$t_{acc} \sim \frac{r}{v_r} \sim r^2/\nu$$

α -Ansatz: $T_{r\phi} = -\alpha p \frac{r}{\Omega} \frac{d\Omega}{dr}$. It follows that

$$\nu = \frac{\alpha c_s^2}{\Omega} = \alpha c_s H$$

c_s : sound speed, H : disk scale height (both include thermal and magnetic pressure).

$$t_{acc} = \frac{1}{\alpha} \left(\frac{t_{cross}}{t_{orb}} \right)^2 t_{orb}$$

Therefore, it takes about $t_{acc}/t_{orb} = \frac{1}{\alpha} \left(\frac{t_{cross}}{t_{orb}} \right)^2$ orbits to drain the disk!

Hartmann et al. (1998) estimate that $\alpha \sim 10^{-2}$ in nearby T Tauri stars.

11.3.2.2 Physical Origins of Disk Viscosity

- viscous mechanism to transport angular momentum and mass
- estimated strength from observations
- what mechanism?

ORDINARY FLUID VISCOSITY

Kinematic viscosity: $\nu = 2\bar{u}\lambda$ \bar{u} : RMS particle speed, λ : mean free path
 protostellar accretion disk:

$$n = 10^{12} \text{ cm}^{-3}, T = 100 \text{ K}, \bar{u} = 0.6 \text{ km s}^{-1},$$

$$\sigma = (1 \text{ nm})^2, \lambda = \frac{1}{n\sigma} = 100 \text{ cm}, \nu \sim 10^8 \text{ cm}^2 \text{ s}^{-1}$$

Let us consider material at a temperature of 100 K that is orbiting 100 AU from a $1 M_{\odot}$ star.

$$c_s = 0.6 \text{ km s}^{-1}, \Omega = 6.3 \times 10^{-3} \text{ yr}^{-1} \Rightarrow \alpha \approx 6 \times 10^{-12} (!)$$

Suppose the gas starts out ~ 100 AU from the star. The time required for the gas to accrete is then

$$t_{acc} \sim \frac{r^2}{\nu} \sim \frac{(100 \text{ AU})^2}{\nu} \sim 10^{22} \text{ s} \sim 10^{15} \text{ yr}$$

Longer than universe!

If that were the only source of angular momentum transport in a disk, then stars would never form. Something else must be at work.

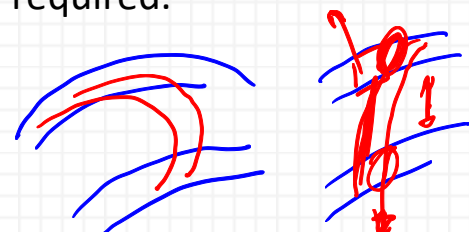
TURBULENT HYDRODYNAMICAL VISCOSITY

If there are large-scale radial motions within a disk, then the effective value of $\bar{u}\lambda$ could be significantly larger than the microphysical one we calculated. In effect, these motions will mix material from different radii within the disk, exchanging angular momentum between inner and outer parts of the disk.

Numerical simulations have been attempted, and seem to find that hydrodynamic mechanisms do not produce significant angular momentum transport, but they may be compromised by limited resolution.

Laboratory experiments can reach Reynolds numbers of $\sim 10^6$, and seem to find negligible transport $\alpha < 10^{-6}$ (Ji et al., 2006). Given these results, most researchers are convinced that purely hydrodynamic mechanisms cannot explain the observed lifetimes and rates of angular momentum transport in disks. Instead, some other mechanism is required.

MAGNETO-ROTATIONAL INSTABILITY



- The basic idea is that magnetic field lines threading the disk connect annuli at different radii.
- As the disk rotates and the annuli shear, this stretches the magnetic field line connecting them.
- This causes an opposing magnetic tension, which attempts to force the two points to stay close together, and thus to force them into co-rotation.
- This speeds up the outermost fluid element, which is falling behind, and slows down the innermost one, and thus it moves angular momentum outward.
- However, when you remove angular momentum from a fluid element it tends to fall toward the center, so the innermost fluid element falls even closer to the star.
- Similarly, the outermost fluid element gains angular momentum, and so it wants to move outward.
- This increases the tension even more, and the system goes unstable due to this positive feedback loop.

Simulators are still working to try to come up with a general result about the value of α produced by the MRI, but in at least some cases a as high as 0.1 seems to be possible.

Problem:

- MRI will only operate as long as matter is sufficiently coupled to the magnetic field

GRAVITATIONAL TRANSPORT MECHANISMS

Gravitational Instability: Toomre parameter Q :

$$\dot{M} = \frac{3\alpha c_s^3}{Q G}$$



If $Q > 1$ (grav. stable), and $\alpha < 1$ maximum rate at which the disk can move matter $\sim c_s^3/G$.

This is also the characteristic rate at which matter falls onto the disk from a thermally-supported core, provided that we use the sound speed in the core rather than in the disk.

- ⇒ in any regions where the disk is not significantly warmer than the core that is feeding it (e.g. the outer parts of the disk where stellar and viscous heating are small), the disk cannot transport matter inward as quickly as it is fed.
- ⇒ the surface density will rise and Q will decrease, giving rise to gravitational instability. |
- ⇒ This can in turn generate transport of angular momentum via gravitational torques.
- ⇒ The disk can also transfer angular momentum to the star by forcing the star to move away from the center of mass. In this configuration the disk develops a one-armed spiral, and the star in effect goes into a binary orbit with the over-density in the disk.
- ⇒ This phenomenon is known as the Sling instability Shu et al. (1990).

11.3.3 Outflow Launching

How and why disks launch the ubiquitous jets and winds that observations reveal.

Driving mechanism?

Stellar winds?

- High pressure in solar corona drives gas outward: mechanical luminosity: $\sim 10^{-4} L_{\odot}$ |
- Observed outflows from young stars: $\sim 0.1 L_{\odot}$ |
- No!

Photon pressure?

- stellar photon field does not have enough momentum to drive the observed outflows of young stars

Neither the thermal winds of low mass main sequence stars, nor the radiatively-driven winds of massive ones, show highly collimated features like the HH jets.

Most natural mechanism: gravitational potential energy being liberated by the accretion flow, which, combined with magnetic fields, can produce highly collimated outflows.

